**Atmospheric
Chemistry
and Physics
Discussions**

Improved radiation
scheme in a GCM

C. Cagnazzo et al.

Printer-friendly Version

Interactive Discussion

EGU

Impact of an improved radiation scheme in the MAECHAM5 General Circulation Model

C. Cagnazzo[1], E. Manzini[1], M. A. Giorgetta[2], and P. M. De F. Forster[3]

[1]Istituto Nazionale di Geofisica e Vulcanologia, Bologna, Italy
[2]Max Planck Institute for Meteorology, Hamburg, Germany
[3]School of Earth and Environment, University of Leeds, UK

Correspondence to: C. Cagnazzo (cagnazzo@bo.ingv.it)

Abstract

In order to improve the representation of the shortwave radiative transfer in the MAECHAM5 general circulation model, the spectral resolution of the shortwave radiation parameterization used in the model has been increased and extended in the UV-B and UV-C bands. The upgraded shortwave parameterization is first validated offline with a 4 stream discrete-ordinate line-by-line model. Thereafter, two 20-years simulations with the MAECHAM5 middle atmosphere general circulation model are performed to evaluate the temperature changes and the dynamical feedbacks arising from the newly introduced parameterization. The offline clear-sky comparison of the standard and upgraded parameterizations with the discrete ordinate model shows considerable improvement for the upgraded parameterization in terms of shortwave fluxes and heating rates. In the simulation with the upgraded ratiation parameterization, we report a significant warming of almost the entire atmosphere, largest at 1 hPa at the stratopause, and stronger zonal mean zonal winds in the middle atmosphere. The warming at the summer stratopause alleviates the cold bias present in the model when the standard radiation scheme is used. The stronger zonal mean zonal winds induce a dynamical feedback that results in a dynamical warming (cooling) of the polar winter (summer) mesosphere, caused by an increased downward (upward)circulation in the winter (summer) hemisphere. In the troposphere, the changes in the spectral resolution and the associated changes in the cloud optical parameters introduce a relatively small warming and, consistenly, a moisteneing. The warming occurs mostly in the upper troposphere and can contribute to a possible improvement of the model temperature climatology.

1 Introduction

Solar radiation is the fundamental energy source for atmospheric motions. A proper representation of radiative transfer in atmosphere General Circulation Models (GCMs)

has therefore always been a necessary condition for a correct simulation of the modelled energy content of the planet. Radiative transfer parameterizations for GCMs have indeed been among the first parameterizations to be developed to a high degree of complexity and to be the subject of systematic and intensive validations. See for instance the recent work by Halthore et al. (2005) and references therein. Many issues related to radiative transfer that are now under investigation, generally focus on the treatment of clouds and aerosols. Another aspect, that may have not received so much attention, is the representation of radiative transfer in the middle atmosphere. Within the GRIPS (GCM Intercomparison for SPARC, Stratospheric Processes and their Role in Climate) project, the first intercomparison of middle atmosphere GCMs showed a general cold bias in the global averaged temperature (Pawson et al., 2000), indicative of systematic uncertainties in the radiative transfer parameterizations used in the models. More recently, part of the Chemistry Climate Model Validation (CCMVAL, Eyring et al., 2005) exercise aims to help understand model differences by comprehensively evaluating the radiative parameterizations employed in the models.

The purpose of this work is to upgrade the shortwave radiative parameterization of a middle atmosphere GCM, with the aim to improve the simulated climatological temperature. The approach we follow is to implement new bands in the parameterization that is already in the middle atmosphere GCM. The radiative transfer within these new bands therefore is calculated for the entire atmosphere, namely between the top of the model and the Earth's surface. Consequently, this approach needs to include a modification of the treatment of the cloud optical properties. We follow this approach for its comprehensiveness.

The middle atmosphere GCM considered is the MAECHAM5 model (Manzini et al., 2006). Previous work, based on an earlier cycle of the model, indicated that the modelled temperature structure is affected by a cold bias that is largest in the tropics and summer hemisphere of the upper stratosphere. Manzini and McFarlane (1998) found an average cold bias in the summer hemisphere of −5 K to −15 K that was independent on the parameterization of gravity waves. Subsequently, in coupled applications

EGU

of the MAECHAM4 model with chemistry models, both Steil et al. (2003) and Egorova et al. (2005) found an average cold bias ranging between –4 K to –8 K between 30° S and 30° N in the upper stratosphere with respect to 9 years of HALOE temperatures (Steil et al., 2003) and an average of re-analysis data (Egorova et al., 2005). Given the coarse spectral resolution of the solar radiation scheme in the UV-visible spectrum, a plausible reason for this cold bias is an underestimation of ozone absorption in the middle atmosphere of the model. Although many aspects of the MAECHAM5 model are new or modified with respect to its predecessor MA-ECHAM4, the treatment of the UV-visible bands has not changed. Therefore, it is of interest to investigate the effect of changes to the UV-visible band treatment in the model. Given our aim to use the same radiation parameterization for the full atmosphere, we follow the upgrade from 4 to 6 bands of the solar radiation parameterization implemented in the ECMWF model (Morcrette et al., 2001; Iacono et al., 2002). Firstly, we report the validation of the 6-band parameterization with respect to the 4-band parameterization against a 4 stream discrete-ordinate line-by-line model. Secondly, we implement the 6-band parameterization in the MAECHAM5 model and compare results with a control simulation employing the 4-band parameterization.

In Sect. 2 the models, the parameterization and the methodology are introduced. Section 3 validates the 6-band parameterization with the discrete-ordinate model. The radiative and dynamical responses of the GCM to the changes in the solar radiation parameterization are presented in Sect. 4, focusing on the middle atmosphere and the troposphere.

2 Model and Methodology

The MAECHAM5 model used in this work is the latest version (Manzini et al., 2006) of the middle atmosphere GCM based on the ECHAM model suite (Roeckner et al., 2006). Concerning gravity wave parameterizations, the MAECHAM5 model includes an orographic gravity wave drag parameterization (Lott and Miller, 1997) and the Hines

Improved radiation scheme in a GCM

C. Cagnazzo et al.

Title Page

Abstract	Introduction
Conclusions	References
Tables	Figures

| ◄◄ | ►► |
| ◄ | ► |

| Back | Close |

Full Screen / Esc

Printer-friendly Version

Interactive Discussion

EGU

parameterization of the momentum flux deposition from an atmospheric gravity wave spectrum (Hines, 1997). The source spectrum of the Hines parameterizations is as specified in Manzini et al. (2006).

2.1 Radiation Parameterizations

Aspects of the radiation parameterization and its validation are described in Roeckner et al. (2003) and Wild and Roeckner (2006), respectively. The standard spectral resolution of the solar radiation parameterization is 4 bands (referenced here as SW4, see Table 1), with 1 band for the UV and visible (250 to 690 nm) and three bands for the near-infrared (690 to 4000 nm). The parameterization follows the approach of Fouquart and Bonnel (1980). It includes absorption by water vapour and ozone, both varying in time and space, and CO_2, N_2O, CO, CH_4 and O_2 as Uniformly Mixed Gases (UMG), and Rayleigh and aerosol scattering. Absorbing gases are also indicated in Table 1.

he SW parameterization has been upgraded by increasing its spectral resolution from 4 to 6 bands. The 6-band version of the radiation parameterization (hereinafter SW6) kindly provided by ECMWF (Morcrette et al., 2001) has been implemented and adapted to the MAECHAM5 model (see Table 1). The upgrade subdivided the 250–690 nm interval and added an extra band in the ultraviolet from 185 to 250 nm, creating a total of three bands in the UV-visible spectral range (185–250 nm, 250–440 nm and 440–690 nm) and three bands for the Near-Infrared (690–1190 nm, 1190–2380 nm and 2380–4000 nm). The extension to 6 bands has been performed in a consistent manner, so that the SW6 parameterization is used throughout the atmosphere (between the top of the atmosphere and the surface). Therefore, the optical properties for water and ice clouds had to be changed. In the current implementation of the SW6 parameterization, the Fouquart et al. (1987) and Ebert et al. (1992) derivations for the optical proprieties have been used, respectively for the water and ice clouds, following (Morcrette et al., 2001).

2.2 Design of the simulations

Two 20-year simulations have been performed with the MAECHAM5 model: The first simulation (hereafter CTRL) with the SW4 (standard) parameterization and the second simulation (hereafter EXP) with the SW6 parameterization. Both simulations use T42 horizontal truncation and 39 vertical levels from the surface to 80 km (0.01 hPa). This model configuration is the one also used in Manzini et al. (2006). The simulations are performed with climatological sea surface temperatures (AMIP2), specified ozone climatology and greenhouse gases (GHG) for the 1990s (see Manzini et al., 2006, for details).

3 Offline validation of SW6

he stand-alone performance of the SW6 and SW4 parameterizations is here assessed by comparison with a sophisticated offline radiation model. This offline code is a Discrete-Ordinate 4 stream scattering model (Stamnes et al., 1998) coupled to the line by line Reference Forward Model (RFM, Dudhia, 1997). It has previously been used at the University of Reading as a reference calculation for GCM radiation schemes and found to be in excellent agreement with other line by line models (see Collins et al., 2006); this model is referred to here as LBL. As in Collins et al. (2006) comparisons are made employing a single mid-latitude summer profile in offline calculations that assume a clear-sky and aerosol-free atmosphere.

Clear-sky shortwave fluxes and heating rates were calculated by LBL, SW6 and SW4. Fluxes are shown in Table 2 for the top of the atmosphere (TOA) and the surface. The fluxes are integrated over 185–4000 nm (SW6), 200–3333 nm (LBL) and 250–4000 nm (SW4) spectral regions. These calculations were for a mid-latitude summer temperature, ozone and water vapour profile, with a surface albedo of 0.1, a 60° solar zenith angle, and using specified greenhouse gases (GHG) concentrations from Table 3. The TOA downward fluxes are the same by construction (all schemes use

[ACPD](#)

6, 11067–11092, 2006

Improved radiation scheme in a GCM

C. Cagnazzo et al.

Title Page

Abstract	Introduction
Conclusions	References
Tables	Figures

◄◄   ►►

◄   ►

Back   Close

Full Screen / Esc

Printer-friendly Version

Interactive Discussion

EGU

the same solar zenith angle and solar constant of 1349 Wm^{-2}) compensated for wave-length range difference. At the TOA SW6 and SW4 upward and net fluxes are in agreement with LBL, in fact they are within 1.5 Wm^{-2} of the fluxes calculated by the LBL model. The SW4 downward surface flux is 15.3 Wm^{-2} larger than that from the LBL, therefore overestimating the amount of radiation arriving at the surface. The difference in the downward surface flux is reduced by about an order of magnitude for the SW6 with respect to the LBL (1.2 Wm^{-2}). Slightly more absorption occurs in the atmosphere for the SW6 case compared to both SW4 and the LBL. This occurs mostly in the middle atmosphere, from the first two bands.

Figure 1 shows the vertical profiles of the total clear-sky shortwave heating rates calculated by LBL, SW6 and SW4, as well as the SW6-LBL and SW4-LBL differences. Results indicate that the SW4 radiation scheme underestimate the heating rates with respect to LBL up to –3K/day at the stratopause. The SW6 heating rates are much improved in the stratosphere with an increase compared to SW4 of 1 to 3 K/day above 10 hPa, peaking at 1 hPa. The comparison with the LBL indicates also an improvement in the troposphere (Fig 1, bottom), although of smaller size: heating rates are increased by 0.1–0.3 K/day below 400 hPa. Differences between LBL and SW6 heating rates are maximum at 0.2 hPa, but are still less than 1 K/day. These results are in agreement with a previous validation of the 6-band version of the ECMWF SW model with the rapid radiative transfer radiation model (RRTM) in both clear-sky and cloudy-sky conditions (Iacono et al., 2002).

Therefore, this validation has permitted to introduce the upgraded scheme in MAECHAM5, to improve its representation of the stratosphere in terms of climatological temperature structure.

EGU

4 Radiative and dynamical response in the Middle Atmosphere GCM

4.1 Changes in the middle atmosphere

Figure 2 shows the January zonal mean shortwave heating rate (20-year average) for the EXP simulation and for the EXP-CTRL difference. In the summer hemisphere, the January zonal-mean heating rate is largest (12–16 K/day) at 1 hPa at the South Pole and ranges between 8 and 10 K/day in the mesosphere. The EXP-CTRL difference is always positive and ranges between 0.2 and 1.8 K/day above 10 hPa. The largest difference occurs at 1 hPa south of 60° S. In the summer middle atmosphere the zonal mean January heating rates of EXP are about 12% larger than the CTRL heating rates.

The January zonal mean temperature for EXP, CTRL and the NCEPCPC analysis (1980–1999) are shown in Fig. 3. The temperature difference between EXP and CTRL (Fig. 3, top-right) is positive almost everywhere, ranging between 1 and 3 K in the lower summer stratosphere, 3 K and 7 K above 10 hPa. The maximum of 7 K occurs between 1 and 0.1 hPa, south of 60° S. Above 100 hPa, the difference is always significant south of 60° N. The warmer EXP temperatures are in better agreement with NCEPCPC, especially at the summer hemisphere stratopause. The zonal mean temperature for the CTRL simulation is generally colder than the NCEPCPC analysis. At 1 hPa, south of 60° S, the NCEPCPC January temperatures are up to 290 K, whereas the CTRL temperatures do not reach 280 K. The seasonal cycle of monthly zonal mean temperature differences (CTRL-NCEPCPC) and the (EXP-CTRL) at the stratopause (1 hPa) are shown in Fig. 4. With the exception of the polar regions in winter, the CTRL temperature bias is generally negative. In the tropics and summer hemispheres, the CTRL-NCEPCPC temperature difference ranges typically from 8 to 14 K. This cold bias is substantially reduced in the EXP simulation, as shown by the positive and significant EXP-CTRL temperature difference (Fig. 4, right). Except for polar winter conditions the EXP temperature is 6 to 8 K warmer than the CTRL temperature, throughout the year. The climatological temperature bias at the stratopause is therefore reduced of about a factor 2 for the EXP simulation, in better agreement with the NCEPCCP analysis.

EGU

In summary, Figures 3 and 4 demonstrate that the direct consequence of the increase in the shortwave heating rate (mainly due to increased ozone absorption) is a significant warming of the summer hemisphere and the winter hemisphere, except for the polar night regions. Instead, the warming that occurs in polar night conditions in the winter polar mesosphere (Fig. 4, top right) in SW6 with respect to SW4 cannot be associated with the change in the shortwave heating rates. As it is shown later, this warming, as well as the adjacent patterns of temperature minima and maxima, are understood to be a dynamical response to the changes in the radiation parameterization. The 20 years average of the January zonal mean zonal winds for EXP and for the (EXP-CTRL) difference are shown in Fig. 5 (top). The largest differences in zonal mean zonal wind occur at the stratopause and in the mesosphere, where the temperature differences are larger (Fig. 3 and 4). The significant differences in zonal wind that occur close to the stratopause indicate stronger jets in each hemisphere: Increased easterlies in the Southern Hemisphere (up to 10 m/s) and increased westerlies (up to 8 m/s) in the Northern Hemisphere.

The enhanced easterlies and westerlies for the EXP simulation with respect to the CTRL simulation are a direct radiative response: They are due to the increased North Pole to South Pole temperature gradient (Fig. 3), resulting from the summer hemisphere and tropical radiative warming. Therefore, the direct impact of the change in the radiation parameterization is an enhancement of the climatological solsticial condition in the middle atmosphere. In order to estimate indirect dynamical changes associated with the implementation of the SW6 parameterization, the net shortwave and longwave heating rate for EXP and for the EXP-CTRL difference are shown in Fig. 5 (bottom panels). The EXP net heating rates are positive in the summer hemisphere and negative in the winter hemisphere, implying upward circulation in summer and downward in winter (Andrews et al., 1987). In the mesosphere, the EXP-CTRL net heating rate difference is positive in the summer and negative in the winter hemisphere. Therefore, the climatological circulation in the mesosphere is increased in the EXP simulation with respect to the CTRL. These circulation changes deduced by the changes in the net heating rates

[EGU](#)

indicate that in the mesosphere there is a dynamical response to the implementation of the SW6 parameterization, namely adiabatic cooling by upward motion in summer and warming by downward motion in winter.

These considerations are indeed consistent with the EXP-CTRL temperature difference shown in Fig. 3 (upper right). In the summer hemisphere, the dynamical cooling competes with the strong radiative local warming, reducing it (indeed, the maximum warming of 7 K reduces above 0.1 hPa, even if the heating rates difference ranges between 1.2 and 1.4 K/day in the full mesosphere). In the winter hemisphere, the increased downward motion and the consequent dynamical warming is observed above 0.3 hPa, while below the direct radiative response is seen. Note that Figure 5 shows also additional substructures in the EXP-CTRL net heating rates difference, mainly as a positive/negative difference at 30°N above/below 1 hPa and a positive net heating rate difference north of 60°N, below 1 hPa. These substructures are again consistent with the temperature difference structures shown in Fig. 3.

A plausible explanation for the induced dynamical changes in the mesosphere is a change in the gravity wave filtering in the stratosphere induced by the reported enhancement at the wind jets (Fig. 5 upper left): In the summer/winter stratosphere, stronger easterlies/westerlies at 1 hPa imply an increase of the wind shear at and below the easterly/westerly jet core. At the stratopause, the net momentum flux carried by the gravity waves is thereafter more positive/negative in the summer/winter hemisphere. Above, in the mesosphere, this situation facilitates the deceleration of the easterlies/westerlies in the summer/winter hemisphere leading to an increased circulation (upward in summer and downward in winter). It is not the purpose of the current work to detail this chain of effects, because this behavior of the gravity wave parameterization in the MAECHAM models has been documented and discussed in earlier works (Manzini and McFarlane, 1998; Manzini et al., 2003), although the changes in the background winds arouse for different reasons. The January results are supported by the July temperatures, zonal mean zonal winds and net heating rates (Fig. 6). The July EXP-CTRL temperature difference (Fig. 6 top-right) is very similar to the January

EGU

difference (Fig. 3), but at the South Pole stratopause in the summer hemisphere the difference is larger in January (7 K, Fig. 3) than in July (6 K, Fig. 6). July zonal mean zonal wind differences (Fig. 6 middle-right) are significant near the stratopause, as for January, with increased easterlies in the Northern Hemisphere (up to 8 m/s) and in-
5 creased westerlies south of 50°S (up to 6 m/s). January shortwave heating rates are larger than July heating rates (not shown); a possible reason is that in January the Earth is near the perihelion. Moreover, close to the South Pole (winter hemisphere), a highly significant 6 K difference occurs above the stratopause. As for January, this warming is consistently associated with an increased downward circulation, deduced
10 by the negative net heating rates difference (Fig. 6, bottom-right).

4.2 Changes in the troposphere

In the troposphere, changes in the averaged temperature can be due to both the in-creased spectral resolution and the implementation of a different treatment of the cloud optical proprieties. Given that the focus of this work is on the stratosphere, the impact
15 of the SW6 parameterization on the troposphere is here only briefly reported. Roeck-ner et al. (2006) have documented a general cold bias of the ECHAM5 model in the troposphere which depends on the resolution. For the same horizontal resolution as used here, they find for December–January-February zonal mean temperature differ-ences between ECHAM5 and ERA-40 of –0.5 to –2 K below 200 hPa and –2K to –4K
20 above 200 hPa in the 30°S–30°N region (Fig. 3 top-left of Roeckner et al., 2006).

Figure 7 shows the 20-years average annual and zonal mean EXP SW heating rates, temperature and water vapour fields for the troposphere, together with the annual and zonal mean EXP-CTRL differences. The EXP-CTRL heating rate difference is always positive. Consequentely, also the temperature difference is always positive and it is
25 larger above 400 hPa (greater than 0.5 K). Smaller differences are found for the lower troposphere and close to the surface (0.5–1 K between 400 and 200 hPa; 0–0.5 K be-tween the surface and 400 hPa). The general increase in the heating rate and tem-perature is consistent with the clear sky SW6-LBL comparison for the troposphere.

Therefore, this warming of the troposphere can be attributed to the changes in the radiative proprieties of the middle atmosphere. The smaller scale features appearing in Fig. 7 (for insteance, at the Equator the SW heating rate difference is largest above 300 hPa) are instead consistent with increased ice clouds between 200 and 300 hPa for EXP (3% to 10% at the Equator, not shown)

The EXP-CTRL water vapour difference, in percentage, is always positive, consistently with a warmer troposphere. Below 200 hPa, EXP is about 3% moister than CTRL, in the Southern Hemisphere and in the Northern Hemisphere south of 30° N. North of 30° N, the EXP lower and middle troposphere is 6%–9% moister than CTRL, in agreement with the temperature difference (more pronounced in the Northern than in the Southern Hemisphere). Above 200 hPa, in a relatively dry region, EXP is 12% to 30% moister than CTRL, with largest differences observed at the Equator.

5 Conclusions

The shortwave radiation parameterization has been upgraded following the ECMWF approach, by increasing its spectral resolution from 4 to 6 bands (Morcrette et al., 2001) and changing the optical proprieties of the clouds accordingly. To test the 4 and 6-band radiation parameterization performances, stand-alone comparisons with a LBL model have been carried out. Results show an improvement of the 6-band scheme with respect to the 4-band scheme in terms of SW surface fluxes and heating rates with a significant increase of the heating rates in the entire atmosphere, largest at 1 hPa (+3 K/day). Two 20-years simulations with the MAECHAM5 GCM have been performed, the first with the 4-band scheme (CTRL) and the second with the 6-band version (EXP). In the middle atmosphere, it is found that the shortwave heating rate in the summer hemisphere is larger in EXP than in CTRL (up to 1.8 K/day), following the expectation for the comparison with the LBL.

The direct consequence of the change in the shortwave heating rate is a significant warming of almost the entire middle atmosphere, largest at the summer stratopause

EGU

EGU

and in the mesosphere (5 K to 7 K), leading to an enhancement of the climatological solsticial condition in the middle atmosphere. In comparison with previous model versions, the newly introduced short wave parameterization results in an improvement of the climatological modelled temperature in the upper stratosphere.

5 The EXP-CTRL warming of the middle atmosphere has the following dynamical consequences: 1. Direct radiative response:

The enhanced winter to summer pole temperature gradient at the stratopause produces stronger easterlies (westerlies) in the summer (winter) hemisphere, in the middle atmosphere. The changes in the winds are largest at the stratopause.

10 2. Indirect dynamical response caused by the enhanced wind jets:

Dynamical cooling occurs in the polar summer mesosphere and dynamical warming in the polar winter mesosphere. While the former is masked by direct radiative warming, the latter dominates the temperature response in both January and July. The indirect dynamical response can be understood as a change in the gravity wave filtering in the

15 stratosphere induced by the direct radiative response in the zonal mean winds and is consistent with the reported changes in the net heating rates.

In the troposphere, an annual mean warming of 0.5 K is found in the middle troposphere and a warming of 1 to 1.5 K in the upper troposphere. Consistently with the warming, on annual average the troposphere shows a moistening (3% to 9% in the mid-

20 dle troposphere, 12% to 30% above 200 hPa). With respect to Roeckner et al. (2006), the temperature difference in the troposphere therefore indicates an improvement of the modelled climatology for the SW6 parameterization.

It is important to note that the current results, although significant, are limited by the specification of the ozone distribution in the model. Namely, an atmosphere model with

25 fixed ozone neglects the feedback between temperature and ozone, particularly large in the upper stratosphere. Ultimately, a consistent comparison with satellite data of modelled strospheric temperatures will have to be done with results from Chemistry Climate Models. Therefore, it will be of interest to evaluate the impact of the SW6 parametrization on the stratospheric temperatures of a version of the MAECHAM5

model that is coupled to a chemistry model.

The current study has shown that changes in the radiative properties of the middle atmosphere have had significant impacts on the troposphere, for both the global climatological temperature and water vapour distributions. Close to the Earth's surface, these changes have been mitigated by the imposed sea surface temperatures. In the case of a coupled atmosphere ocean GCM, such changes in the ratiative transfer of the atmosphere would have instead lead to a different climate equilibrium. Therefore, our results point to the importance of including a proper representation of the stratosphere also in coupled atmosphere ocean GCMs.

References

Andrews, D. G., Holton, J. R., and Leovy, C. B.: Middle Atmospheric Dynamics, Academic, San Diego, CA, 1987. 11075

Collins, W. D., Ramaswamy, V., Schwarzkopf, M. D., et al.: Radiative forcing by well-mixed greenhouse gases: Estimates from climate models in the Intergovernmental Panel on Climate Change (IPCC) Fourth Assessment Report (AR4), J. Geophys. Res., 111, D14317, doi:10.1029/2005JD006713, 2006. 11072

Dudhia, A.: RFM v3 software user's manual, Tech. Rep. ESA POMA-OXF-GS-0003, Atmos., Oceanic, and Planet. Phys., Clarendon Lab., Oxford, U. K., 1997. 11072

Ebert, E. E., and Curry, J. A.: A parameterization of cirrus cloud optical properties for climate models, J. Geophys. Res., 97, 3831–3836, 1992. 11071

Egorova, T., Rozanov, E., Zubov, V., Manzini, E., Schmutz, W., and Peter, T.: Chemistry-climate model SOCOL: a validation of the present-day climatology, Atmos. Chem. Phys., 5, 1557–1576, 2005. 11070

Eyring, V., Harris, N. R. P., Rex, M., et al.: A Strategy for Process-Oriented Valida-

EGU

tion of Coupled Chemistry Climate Models, Bull. Am. Meteor. Soc., 86, pp.1117–1133, doi:10.1175/BAMS-86-8-1117, 2005. 11069

Fouquart, Y., and Bonnel, B.: Computations of solar heating of the Earth's atmosphere: A new parameterization, Beitr. Phys. Atmos., 53, 35–62, 1980. 11071

Fouquart, Y., Bonnel, B., Brogniez, G., Buriez, J. C., Smith, L., Morcrette, J. J., and Cerf, A.: Observations of Saharan aerosols: results of ECLATS field experiment. Part II: broadband radiative characteristics of the aerosols and vertical radiative flux divergence, J. Clim. Appl. Meteor., 26, 38–52, 1987. 11071

Halthore, R. N., Crips, D., Schwartz, S. E., et al.: Intercomparison of shortwave radiative transfer codes and measurements, J. Geophys. Res., 110, D11206, doi:10.1029/2004JD005293, 2005. 11069

Hines C. O., Doppler spread parametrization of gravity wave momentum deposition in the middle atmosphere, 1, Basic formulation, J. Atmos. Solar Terr. Phys., 59, 371–386, 1997. 11071

Iacono, M. J., Delamere, J. S., Mlawer, E. J., and Clough, S. A.: Cloudy Sky RRTM Shortwave Radiative Transfer and Comparison to the Revised ECMWF Shortwave Model, Twelfth ARM Science Team Meeting Proceedings, St. Petersburg, Florida, April 8–12, Atmospheric and Environmental Research, Inc. Lexington, Massachusetts, 2002. 11070, 11073

Lott, F., and Miller, M.: A new subgrid scale orographic drag parameterization; its testing in the ECMWF model, Quart. J. Roy. Meteorol. Soc, 123, 101–127, 1997. 11070

Manzini, E., and McFarlane, N. A.: The effect of varying the source spectrum of a gravity wave parameterization in a middle atmosphere general circulation model, J.Geophys. Res., 103, 31 523–31 539, 1998. 11069, 11076

Manzini, E., Steil, B., Bruehl, C., Giorgetta, M. A., and Krueger, K.: A new interactive chemistry-climate model: 2. Sensitivity of the middle atmosphere to ozone depletion and increase in greenhouse gases and implications for recent stratospheric cooling, J. Geophys. Res., 108, 4429, doi:10.1029/2002JD002977, 2003. 11076

Manzini, E., Giorgetta, M. A., Esch, M., Kornblueh, L., and Roeckner, E.: The influence of sea surface temperatures on the Northern winter stratosphere: Ensemble simulations with the MAECHAM5 model, J. Climate, 19, 3863–3881, 2006. 11069, 11070, 11071, 11072

Morcrette, J. J., Mlawer, E. J., Iacono, M. J., and Clough, S. A.: Impact of the radiation-transfer scheme RRTM in the ECMWF forecast system, Technical Report in the ECMWF Newsletter, No. 91, 2001. 11070, 11071, 11078

Pawson, S., Kodera, K., Hamilton, K., et al.: GCM-Reality Intercomparison Project for SPARC:

Title Page

Abstract | Introduction

Conclusions | References

Tables | Figures

◀◀ | ▶▶

◀ | ▶

Back | Close

Full Screen / Esc

Printer-friendly Version

Interactive Discussion

EGU

Scientific Issues and Initial Results, Bull. Am. Meteorol. Soc., 81, 781–796, 2000. 11069

Roeckner, E., Bäuml, G. Bonaventura, L., et al.: The atmospheric general circulation model ECHAM5. Part I: Model description, Max Planck Institute for Meteorology Rep. 349, 2003. 11071

5 Roeckner, E., Brokopf, R., Esch, M., Giorgetta, M., Hagemann, S., Kornblueh, L., Manzini, E., Schlese, U., and Schulzweida, U.: Sensitivity of simulated climate to horizontal and vertical resolution in the ECHAM5 atmosphere model, J. Climate, 2006. 11070, 11077, 11079

Stamnes, K., Tsay, S. C., Wiscombe, W., and Jayaweera, K.: A numerically stable algorithm for discrete-ordinate-method radiative transfer in multiple scattering and emitting layered media, 10 Appl. Opt., 27, 2502–2509, 1998. 11072

Steil, B., Bruehl, C., Manzini, E., Crutzen, P. J., Lelieveld, J., Rasch, P. J., Roeckner, E., and Krueger, K.: A new interactive chemistry-climate model: 1. Present-day climatology and interannual variability of the middle atmosphere using the model and 9 years of HALOE/UARS data, J. Geophys. Res., 108(D9), 4290, doi:10.1029/2002JD002971, 2003. 11070

15 Wild, M. and Roeckner, E.: Radiative fluxes in the ECHAM5 general circulation model, J. Clim., 19, 3792–3809, doi:10.1175/JCLI3823.1, 2006. 11071

◄◄ | ►►

◄ | ►

Back | Close

Full Screen / Esc

Printer-friendly Version

Interactive Discussion

EGU

EGU

Table 1. Spectral intervals and absorbing gases for the SW4 and SW6 parameterizations.

ECHAM5-SW4 bands	Gases	-	ECHAM5-SW6 bands	Gases
		-	185–250 nm	O3
250–690 nm	H_2O, O_3, UMG	-	250 – 440 nm	O_3, UMG
		-	440–690 nm	H_2O, O_3, UMG
690–1190 nm	H_2O, UMG	-	690–1190 nm	H_2O, UMG
1190–2380 nm	H_2O, UMG	-	1190–2380 nm	H_2O, UMG
2380–4000 nm	H_2O, O_3, UMG	-	2380–4000 nm	H_2O, O_3, UMG

EGU

Table 2. TOA and Surface Total fluxes in Wm^{-2}.

Code	TOA Down	TOA Up	TOA Net	-	Surf Down	Surf Up	Surf Net
LBL	674.28	88.4	585.878	-	488.45	48.84	439.60
SW6	674.28	89.89	584.384	-	487.22	49.21	438.00
SW4	674.28	87.98	586.300	-	503.70	50.88	452.82

Table 3. GHG concentrations for comparison with LBL.

GHG gases	Concentration
CO_2	287 ppmv
CH_4	806 ppbv
N_2O	275 ppbv

EGU
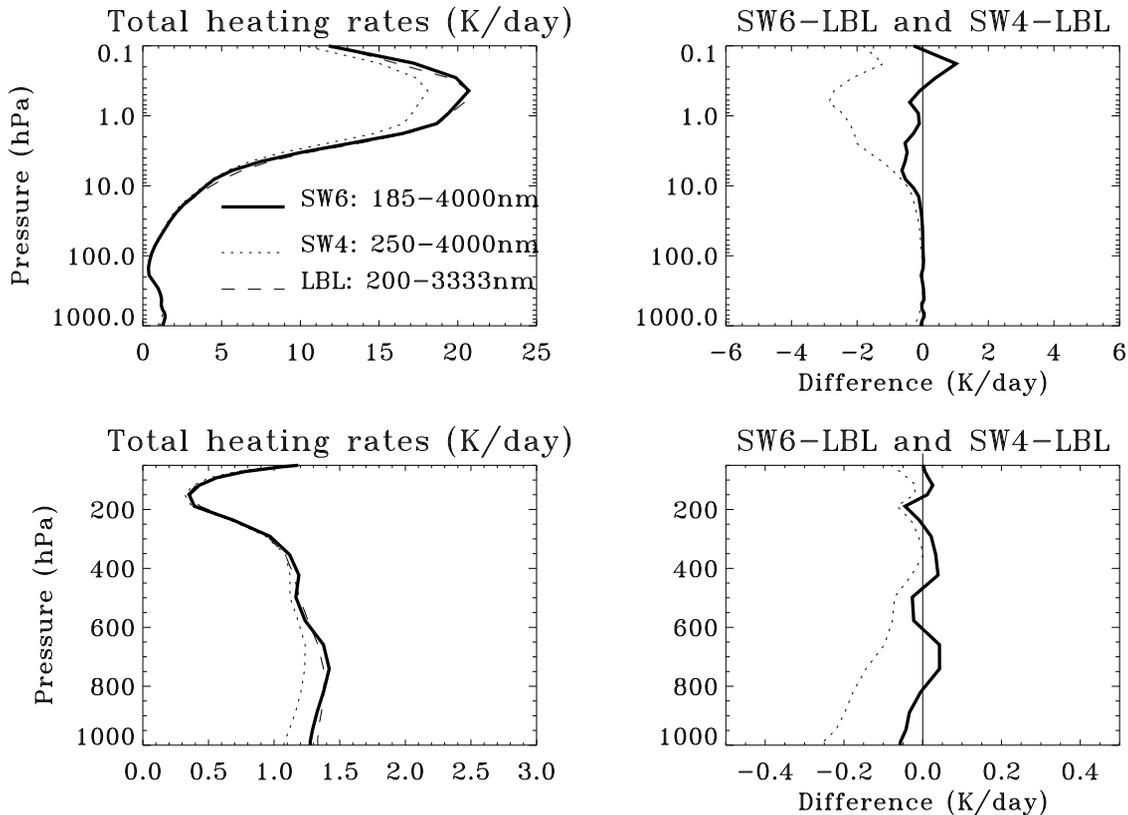
Fig. 1. Vertical profiles of total shortwave (SW) heating rates in K/day. Left: SW6, SW4 and LBL are represented with continuous, dotted and dashed lines, respectively. Right: SW6-LBL (continuous line) and SW4-LBL (dotted line) heating rates differences in K/day. Upper panels: from 1000 to 0.01 hPa in logarithmic vertical scale in pressure; lower panels: from 1000 to 10 hPa, linear vertical scale in pressure.

Improved radiation scheme in a GCM

C. Cagnazzo et al.

Title Page

Abstract	Introduction
Conclusions	References
Tables	Figures

I◄	►I
◄	►
Back	Close

Full Screen / Esc

Printer-friendly Version

Interactive Discussion

EGU
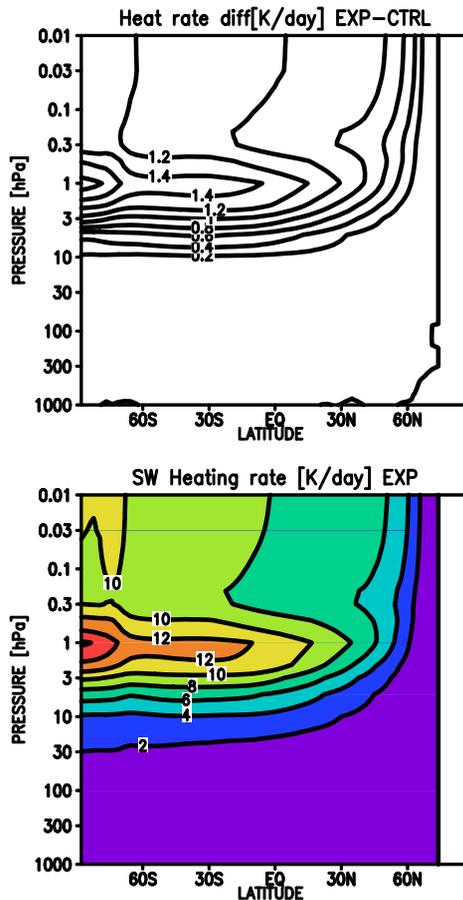
Fig. 2. Top: 20-years average of January zonal mean shortwave (SW) heating rates for the EXP simulation in K/day versus altitude (1000 to 0.01 hPa) and latitude; contour intervals are 2 K/day. Bottom: January heating rates difference (EXP-CTRL) in K/day; contour intervals are 0.2 K/day.

EGU
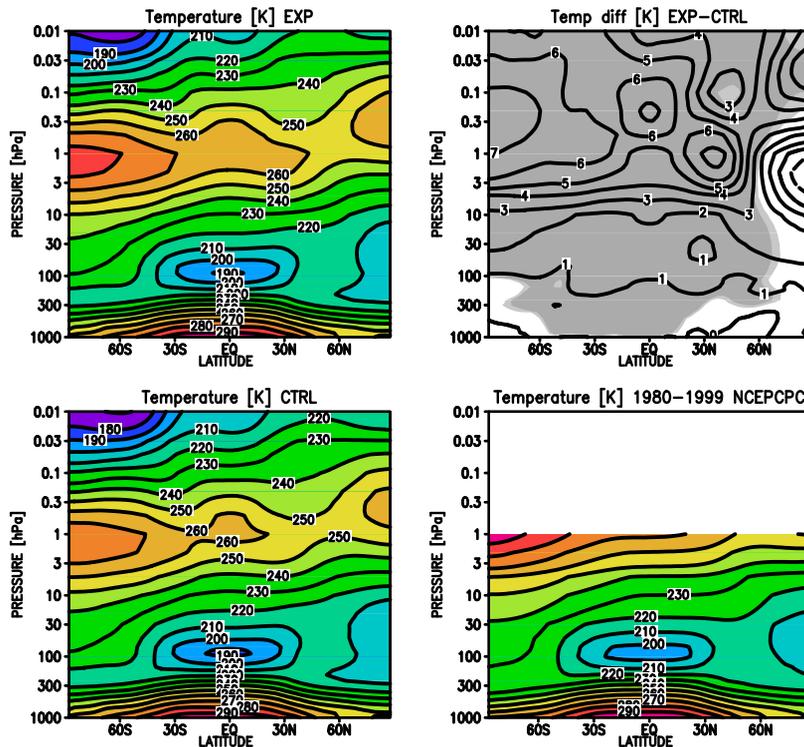
Fig. 3. January zonal mean temperature (20-years average) versus latitude and pressure for the EXP simulation (top-left), the (EXP-CTRL) difference (top-right), the CTRL simulation (bottom-left) and NCEPCPC analysis (bottom-right); units are K and contour intervals are 1 K(top) and 10 K (middle and bottom). Light and dark grey regions are significant at 99% and 95%, respectively with a t-Student test.

EGU
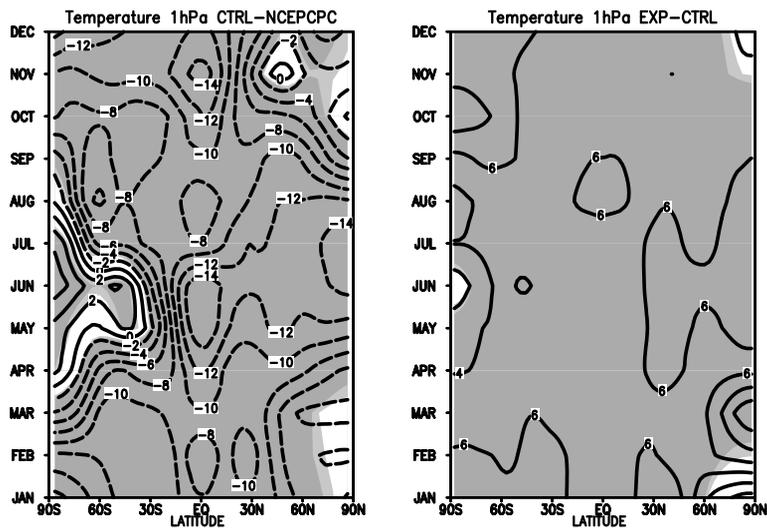
Fig. 4. Latitude-time section of the monthly and zonal mean temperature difference between the CTRL simulation and the NCEPCPC analysis (CTRL-NCEPCPC, left) and between the EXP and the CTRL simulation (EXP-CTRL, right), at 1 hPa (20 years average). Contour interval is 2 K.
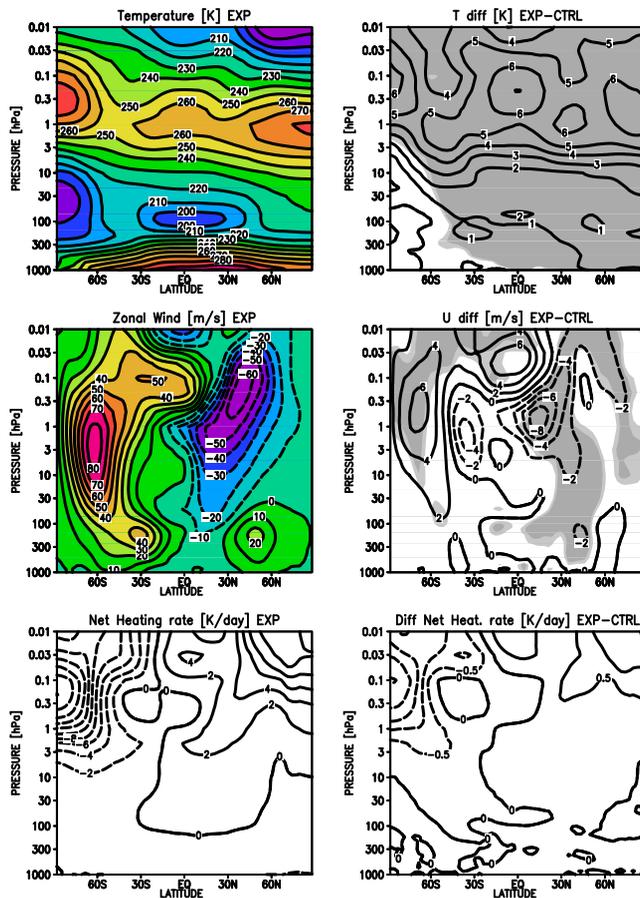
EGU
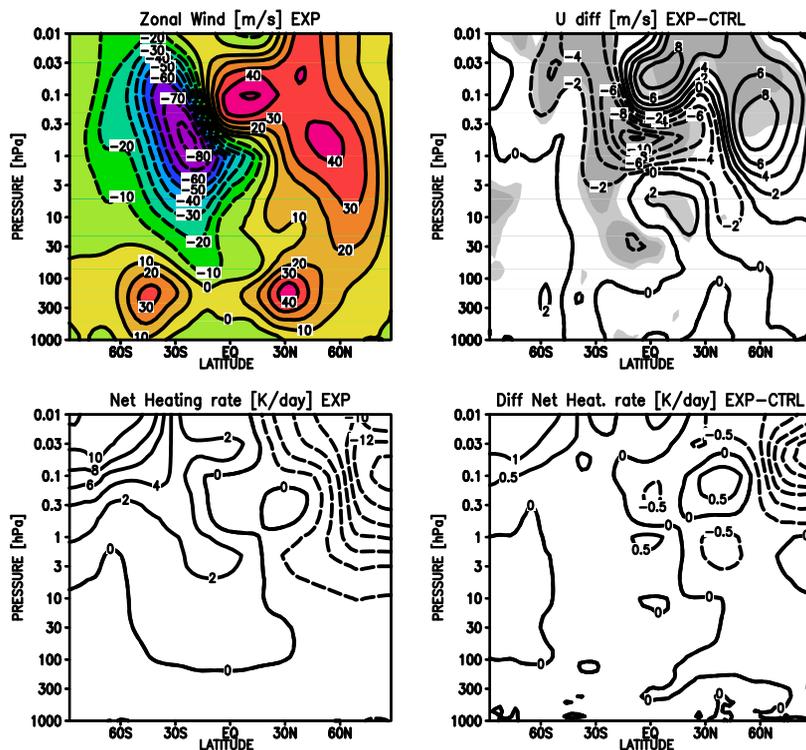
Fig. 5. Top: January (20-years average) zonal-mean zonal-winds versus altitude and latitude for the EXP simulation (left) and the (EXP-CTRL) difference (right); units are m/s and contour intervals are 10 m/s (left) and 2 m/s (right); here after, dashed contour lines represent negative values. Bottom: Altitude-latitude profiles of January net heating rates for EXP (left) and for the (EXP-CTRL) difference (right); units are K/day; contour intervals are 2 K/day (left) and 0.5 K/day (right).

Fig. 6. Top: July zonal mean temperature (20-years average) versus altitude and latitude for the EXP simulation (left) and the (EXP-CTRL) difference (right) in K; middle and bottom: same as Fig. 4, but for July.

EGU
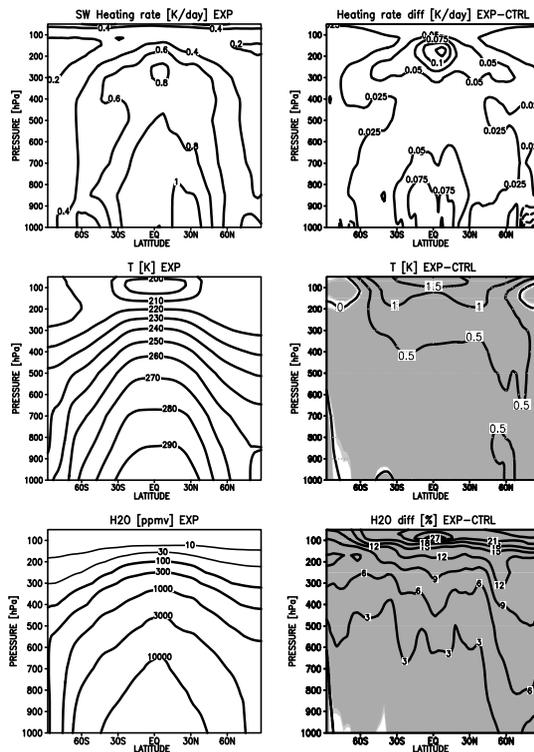
Fig. 7. Latitude-pressure (from 1000 to 50 hPa) contours of 20-years average of the zonal-mean annual-mean: EXP temperature (top-left) and (EXP-CTRL) temperature difference (top-right), in K (contour intervals are 10 K for the temperature and 0.5 K for the temperature difference); Middle: EXP shortwave heating rates (left) and (EXP-CTRL) heating rates difference (right) in K/day; contour intervals are 0.2 K/day (left) and 0.025 K/day (right). Bottom: EXP water vapour (left) and (EXP-CTRL) water vapour difference (right) in ppmv and %; contour intervals are 10 000, 3000, 1000, 300, 100, 30, 10, 3, 1 ppmv (left) and 3% (right).

EGU